JOURNAL OF AIRCRAFT
Vol. 36, No. 6, November–December 1999

Characterization of Fatigue Behavior of Bonded Composite Repairs

John Klug,* Scott Maley,† and C. T. Sun‡
Purdue University, West Lafayette, Indiana 47907-1282

Composite patches are bonded to a cracked metallic surface either symmetrically (double sided) or unsymmetrically (single sided) to extend service life. The stresses in the metallic panel are greatly affected by the repair symmetry. Unsymmetric repairs present the greatest challenge because of the presence of out-of-plane bending. Thermal residual stresses are present because of the thermal coefficient mismatch of the patch and the aluminum plate. Debonding along an adhesive–adherend interface can reduce the patch effectiveness. A simple analysis with Mindlin plate theory is investigated to model the host and the repair plate. The two plates are connected by an adhesive layer modeled by effective springs. Large deflection theory is used in the case of unsymmetric repairs. The springs are ineffective in the debond zone and are removed. Both the aluminum and the debond cracks are characterized by fracture mechanics by use of the stress intensity factor and strain-energy release rate, respectively. Experiments on aluminum 2024-T3 plate, AS4/3501-6 carbon/epoxy composite patch and FM73 adhesive include determining the thermal residual stresses in the aluminum plate and observation of debond development by use of an ultrasonic C-scan. Tests are conducted to examine the metallic and debond crack growth interaction on unsymmetric repairs.

Introduction

TO extend the service life of an aging aircraft, the cracked components must be replaced or repaired. If the number of cracks is small and the crack size is small relative to the size of the component, it is often most economical to use crack arrestment methods to regain the load-carrying capacity of the component. A repair method for which composite patches are used to reinforce the cracked structure has been shown to be very promising, owing to the lightweight, high stiffness, and high strength of the composite.[1]

One of the most challenging aspects of bonded repair technology is stress analysis of the repaired structure. The difficulty arises from the fact that a plane stress metallic panel under in-plane loading develops highly complicated three-dimensional stresses if composite patches are bonded to its surfaces either symmetrically (double sided) or unsymmetrically (single sided). Unsymmetric repairs present the greatest challenge in modeling because of the presence of out-of-plane bending. The two side views, shown in Figs. 1a and 1b, show the bending induced from thermal residual stresses because of the thermal mismatch and from the off-axis loading. Although it has been shown that double-sided repairs exhibit the most effective reinforcement, single-sided repairs provide a clear advantage when it is difficult or impossible to gain access to both sides of a structure.

Many analysis techniques have been proposed.[1–4] However, not much combined analytic and experimental verification has been done at the present time. Perhaps the most extensive work has been done by Baker[5] for double-sided repairs. Predictions of fatigue life are made, including debond effects for many loading conditions. Debond size is destructively examined by removal of the repair at high temperature and examination of the oxidized aluminum surface from the debond zone.

Bending can cause a large variation of the stress intensity factor through the plate thickness. This can lead to curvature of the crack front in thick aluminum plates and makes prediction of the crack growth difficult. Large deflection[6] is expected to play a role in the behavior of the plate when mechanical loading is applied, causing the bending shown in Fig. 1b. The most interesting case is when the mechanical loading is applied after the effects of the thermal residual stresses have been taken into account.

The use of a full three-dimensional finite-element model to perform stress analysis is computationally costly and can even cause ill conditioning when high aspect ratio elements are used for the thin patch and adhesive. In this paper, a simple analysis is investigated by use of Mindlin plate theory to model the host and the repair plates and spring elements to model the connecting adhesive layer. The aluminum crack is characterized by fracture mechanics by use of the stress intensity factor. The distribution of the strain-energy release rate for a debond crack is calculated. A comparison between double- and single-sided repairs with both thick and thin patches is achieved both numerically and experimentally. Fatigue crack growth data is obtained with an ultrasonic C-scan to measure the debond crack nondestructively. An optical microscope is used for the single-sided repair aluminum crack growth. Quantitative comparisons between analysis and experiments are made.

Model and Analysis Description

Figure 2 shows a typical single-sided patch configuration. A complete derivation of the finite-element model is given in Ref. 3. The plate nodes are located on the midplanes of the aluminum plate and patch. The adhesive nodes lie along the patch–adhesive and adhesive–aluminum plate interfaces. Constraint equations are imposed on the patch–adhesive and the adhesive–aluminum interfaces to enforce compatibility. The adhesive layer is modeled by three springs: one in each of the x and the y directions for the transverse shear stiffness in the xz and the yz planes and one in the z direction for the axial stiffness in the z direction.

The modified crack closure technique[7] is used to calculate the strain-energy release rate. It is assumed that the strain energy released during crack extension is equal to the work needed to close the opened crack surfaces. It is also assumed that the adhesive cracks along the aluminum crack region. Generally, the nodal forces and relative displacements from the geometric nonlinearity are nonlinear; therefore the energy required for closing the crack front is the summation of the work done for each increment. However, it has been found that the relation between the nodal forces and relative displacements is linear at the crack tip. Thus, the work done for each increment is linear, and a single-step closure approach can be taken.

Received 15 July 1998; revision received 4 February 1999; accepted for publication 23 February 1999.

*Graduate Student, School of Aeronautics and Astronautics; currently at Aerospace Corporation, El Segundo, CA, 90009.

†Graduate Student, School of Aeronautics and Astronautics. Student Member AIAA.

‡Neil A. Armstrong Distinguished Professor, School of Aeronautics and Astronautics. Fellow AIAA.

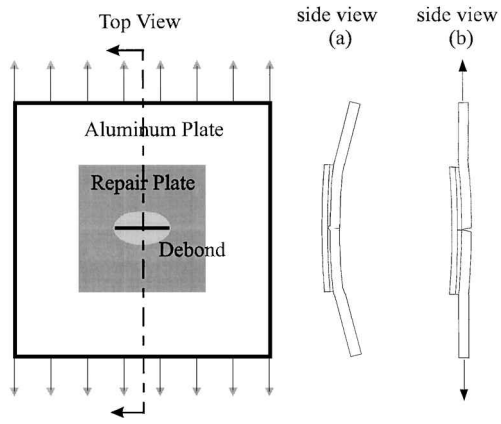

Fig. 1 Curvature of single-sided repair that is due to a) thermal residual stresses and b) mechanical loading.

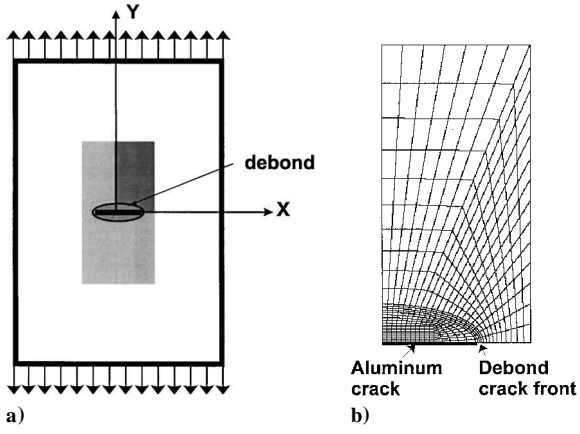

Fig. 2 Configuration of a) a repaired center crack with debond and b) a finite-element mesh with debond (quadrant of patch region shown).

In this case, the strain-energy release rate is computed for mode I fracture loading, but the same procedure can also be used for mixed-mode loading. Four-node Mindlin plate elements (S4R) are used to model the aluminum plate and repair. Figure 3 shows a two-dimensional finite-element model for the aluminum plate near the crack tip at point b. Assume that the crack front extends from b to c. Since the extension Δa is very small, the crack opening displacements at b are taken to be the same as those at a. Thus, the strain-energy release rate can be calculated as the work done by the nodal force and the moments, F_y^b and M_x^b, respectively, in closing the crack opening displacement and rotations u_y^a and ψ_y^a, respectively. The total strain-energy release rate is obtained as

$$\bar{G}_{\text{total}} = \bar{G}_u + \bar{G}_\psi = (1/2\Delta a)\left[F_y^b\left(u_y^a - u_y^{a'}\right)\right] + (1/2\Delta a)\left[M_x^b\left(\psi_y^a - \psi_y^{a'}\right)\right] \quad (1)$$

where $\bar{G}_u$, $\bar{G}_\psi$, and $\bar{G}_{\text{total}}$ are the transitional, rotational, and total strain-energy release rates, respectively. Note that these strain-energy release rates are the respective energies released (over the total plate thickness) per crack tip.

The fracture parameter for the aluminum crack is often given in terms of the stress intensity factor. Because we are looking at a single-sided patch configuration, the stress intensity factor is not uniform through the thickness of the plate. The maximum stress intensity factor is located on the tension side of the plate and is composed of

$$K_I = K_u + K_\psi\left(\frac{2z}{t_s}\right) = \sqrt{\frac{\bar{G}_u E_s}{t_s}} + \sqrt{\frac{3\bar{G}_\psi E_s}{t_s}}\left(\frac{2z}{t_s}\right) \quad (2)$$

Cracking along the bond line is a key mode of failure in patch repair. The debond crack may propagate in either the adhesive–aluminum or the adhesive–patch interface. To predict debond crack growth behavior, the strain-energy release rate along the crack front must be evaluated. The present double-plate model can be used to perform this task.

The debond crack always initiates from the location of the original crack in the aluminum plate. From experimental results, we assume that the debond crack lies in the adhesive–repair plate interface. In fact, when the present plate model is used in conjunction with linear springs to represent the adhesive, the strain-energy release rates for the two possible debond cracks turn out to be identical. The difference in fracture toughness of these two interfaces would determine the actual location of the debond crack.

To illustrate the procedure for calculating the strain-energy release rate, we consider a small region in the neighborhood of the debond crack front. Figure 4 shows part of the finite-element model that includes four (four-noded) plate elements for the aluminum plate and nine spring nodes (a_j^3, b_j^3, and c_j^3, $j = 1, 2, 3$). The debond crack front is at the line $b_1b_2b_3$. The top nodes b_j^3 and c_j^3, which represent the lower edge of the adhesive, are tied by the constraint equations to the corresponding bottom nodes b_j^4 and c_j^4, respectively, which represent the top edge of the aluminum plate. The two sets of nodes a_j^3 and a_j^4 are not constrained because the debond crack has already propagated through this area. The constraints result in reaction forces, N_x, N_y, and N_z and moments M_x and M_y, at these nodes. Note that the spring nodes have only reaction forces. The reaction forces and moments at a node are equal to the respective sums of the nodal forces and moments of all of the elements sharing this node.

The debond crack closure energy can be determined with the assumption that the crack front extends from the current location b_j^3–b_j^4 to c_j^3–c_j^4. As with the previous example of crack closure, the extension Δa is very small and the crack opening displacements at b_j^3–b_j^4 are taken to be the same as those at a_j^3 and a_j^4 before the assumed crack extension. Thus the crack closure energy associated with a pair of nodes (say, b_2^3 and b_2^4) can be expressed in the form

$$2U_{b_2} = N_x^3\Delta u_x^3 + N_y^3\Delta u_y^3 + N_x^3\Delta u_x^3 + N_x^4\Delta u_x^4 + N_y^4\Delta u_y^4 + N_z^4\Delta u_z^4 + M_x^4\Delta\psi_x^4 + M_y^4\Delta\psi_y^4 \quad (3)$$

where N_i^3, N_i^4, and M_i^4 are nodal constraining forces and moments before crack extension at nodes b_2^3 and b_2^4, and u_i^3, u_i^4, and ψ_i^4 are

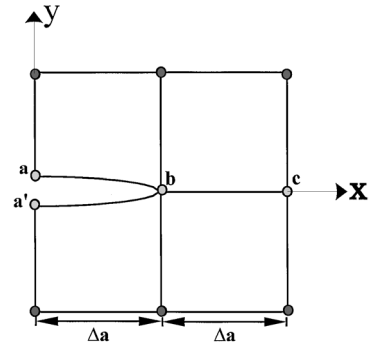

Fig. 3 Aluminum plate crack tip elements (top view).

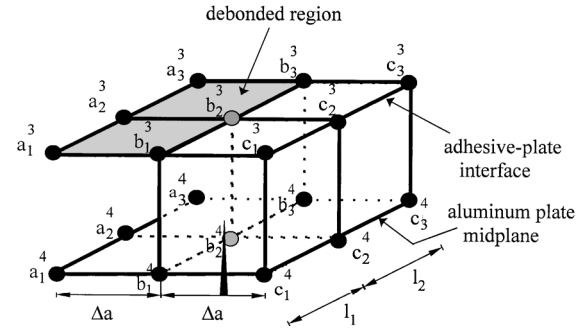

Fig. 4 Schematic of debond crack front.

the nodal displacements and rotations at nodes a_j^3 and a_j^4. In addition, Δu_i^3 denotes the difference of the nodal displacements between nodes a_j^3 and b_j^3, and Δu_i^4 denotes the relative displacements between nodes a_j^4 and b_j^4.

The strain energy released over an area associated with the assumed crack extension can be calculated with Eq. (3). The average strain-energy release rate is obtained by dividing the total strain energy released by the local area. For example, the total strain-energy release rate at b_2 is calculated as

$$G = U_{b_2} \Big/ A \tag{4}$$

where

$$A = \Delta a \frac{(l_1 + l_2)}{2}$$

where l_1 and l_2 are the width of the elements shown in Fig. 4. However, the accuracy of such a calculation depends on the finite-element mesh, especially at the crack front.

The material properties for the graphite/epoxy repair (AS4/3501-6) are shown in Table 1, and the material properties for aluminum and FM73 adhesive are shown in Table 2. Two thicknesses of composite repairs are chosen for comparison of both the single- and the double-sided repairs. Both four-ply (0.508-mm) and eight-ply (1.016-mm) repairs are used. The aluminum sheet thickness t_s and adhesive thickness are 3.1 and 0.10 mm, respectively. Note that the thicknesses and geometry of the repair may not be typical for a design for the given aluminum thickness. Typically, the product of the repair thickness and effective modulus is greater than the product of the modulus and thickness of the metallic structure. Also, the repair edge is tapered and the corners are rounded to reduce the adhesive stresses.[1,8] For this study, it is assumed that the repair is long enough for us to ignore debonding along the untapered boundary.

The first step in analysis is to determine the effect of the thermal residual stresses. Conventionally, the value of the temperature drop, ΔT, is taken as the difference in the ambient room temperature of the component and the curing temperature. For a typical adhesive like FM 73, the curing ΔT temperature is 120°C and the ambient room temperature is 20°C, making a ΔT of −100°C. However, the actual value of ΔT is not well defined because of such things as the adhesive's not hardening at 120°C. Because of this uncertainty, an effective temperature drop ΔT_{eff} is proposed and is defined as the temperature drop that can be adopted in a model without using temperature-dependent material properties.

Two methods of determining this effective temperature drop have been proposed. The first method consists of curing an uncracked panel of composite/adhesive/aluminum to create thermal residual stress. After curing, a strain gauge is placed at the center of the composite panel and an initial strain reading is measured. Subsequently, the aluminum is dissolved with caustic NaOH solution. This method allows removal of the aluminum without the introduction of any additional stresses or temperature effects from grinding. After removal of the aluminum, a strain measurement is again taken. Since the composite plate is no longer constrained by the aluminum plate, the difference in strain measurements is directly related to the amount of residual stress present after patching. This strain is matched to the strains from a finite-element model at varying ΔT. This method can be used for both single- and double-sided patch configurations. For single-sided repairs, there is an additional method available. The residual stresses in a single-sided specimen will cause curvature that can be measured by a three-dimensional coordinate measuring machine. As with the strains, these curvatures can be matched with a finite-element model to determine the effective ΔT. For this analysis ΔT_{eff} is taken to be −70°C.

Only one half of the single-sided and one quarter of the double-sided repairs need to be modeled because of symmetry. Initially, the boundary conditions for the repair and the aluminum plates are free, and the temperature is decreased to model the thermal residual stresses because of cure. Next, the boundary at $y = L_s$ (half the aluminum sheet length) is clamped to model the grip condition. Finally, the load is increased to the maximum stress $\sigma_{\max}$. The displacements at the grip are also constrained to be equal during the loading.

Table 1 Composite material properties

Property	Graphite/epoxy
E_1 (GPa)	138
E_2 (GPa)	9.7
E_3 (GPa)	9.7
G_{12} (GPa)	6.9
G_{13} (GPa)	6.9
G_{23} (GPa)	3.2
ν_{12}	0.3
ν_{13}	0.3
ν_{23}	0.49
$\alpha_1 (10^{-6}\,^\circ\text{C}^{-1})$	−0.7
$\alpha_2 (10^{-6}\,^\circ\text{C}^{-1})$	27.0
$\alpha_3 (10^{-6}\,^\circ\text{C}^{-1})$	27.0

Table 2 Aluminum and adhesive material properties

Property	Aluminum 2024-T3	Adhesive FM 73
E (GPa)	72.0	2.15
ν	0.3	0.4
$\alpha (10^{-6}\,^\circ\text{C}^{-1})$	23.0	——

Specimen Preparation

Figure 5 shows the geometry of the reinforced edge-cracked specimen. The aluminum alloy and the composite repair are 2024-T3 and AS4/3501-6 graphite/epoxy, respectively. Before bonding, the edge crack is initiated with a jeweler's saw (0.008-in. blade). A fatigue crack is then propagated to a total crack length of approximately 13 mm. Note that the edges of the repair are not stepped and will thus give high edge stresses. The specimen is next prepared for the high-temperature bonding.

One of the most critical steps in the bonding procedure is the aluminum surface preparation. Reference 1 details the required steps of the aluminum preparation and are briefly summarized as follows:

1) Surface degreasing: The aluminum surface of the repair area is thoroughly cleaned with methyl ethyl ketone.

2) Abrasion: The repair area is abraded with aluminum oxide abrasive paper to remove the oxide layer and expose a reactive metal surface.

3) Primer: A 1% solution of silane primer (gamma-glycidoxypropyltrimethoxy silane) is brushed onto the repair area for 10 min. The specimen is then air dried. The surface of the composite patch is only degreased and abraded.

Curing of the adhesive is done immediately following the aluminum surface treatment, at 120°C for 1 h. FM 73 (American Cyanamid) adhesive film is used for bonding. Note that the composite is cured before the adhesive bonding cycle.

Fatigue Results and Discussion

The results include numerical results from finite-element analysis and fatigue tests of both single- and double-sided repairs. Ultrasonic C-scans are taken of the repair area to show debonding with varying amounts of fatigue. A through-transmission technique with an immersion tank is used to detect the debonding. Two 10-MHz

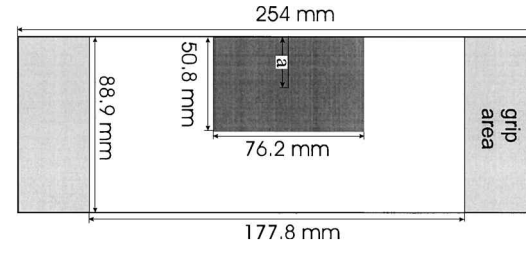

Fig. 5 Geometry of composite repair.

transducers with a 38.1-in. focal length are used. Fatigue tests are performed on a 250 KN MTS testing machine and crack length for single-sided repairs is measured by an optical microscope.

It is well understood that the single-sided repair can affect the global geometry of a cracked structure because of thermal residual stresses that arise from bonding the composite patch at elevated temperatures and from a mechanical in-plane load, as shown in Fig. 1. The effects of this geometrical change on the aluminum crack structure are not simple. In fact, large deflection theory may be required for solving the problem.[6] Figure 6 shows the curvature of the midplane of the aluminum plate along the y axis for the eight-ply repair for both linear and nonlinear, or large deflection theory, analyses with $\Delta T = -70^{\circ}$C. Initially, the plate is curved because of the thermal residual stresses. As the in-plane mechanical load is increased, the plate flattens. Further increase of the load causes the plate to curve in the opposite direction. The plot shows that for this geometry there is little difference between the nonlinear and the linear analysis.

Figure 7 shows the normalized stress intensity factor at the aluminum plate midplane K_m and free surface K_f vs the applied stress for both the nonlinear and the linear solutions. The aluminum crack length is 12.7 mm. The stress intensity factor is normalized by the plane strain critical value K_{Ic} for aluminum 2024-T3. The data are shown for $\Delta T = -70^{\circ}$C, and there is little difference between the linear and the nonlinear solutions. Interestingly, the magnitude of the stress intensity factor is approximately the same for the four- and the eight-ply repairs. However, at high loads the stress intensity factor for the four-ply is slightly higher than that for the eight-ply repair. At zero load, the eight-ply repair stress intensity factor is higher because of greater thermal residual stresses. Also note that the stress intensity factor at zero load is larger at the midplane. This is due to bending stresses in the aluminum plate that arise from the thermal residual stresses. The maximum value of the stress intensity factor is at the aluminum–adhesive interface rather than at the free surface of the aluminum plate. For instance, for a cyclic stress from 0 to 10 MPa, the maximum value of the stress intensity factor will also shift from the aluminum–adhesive interface to the free surface of the plate.

The double-sided repair results for both repair thicknesses are shown in Fig. 8. The stress intensity factor is higher for the thicker repair at zero load when thermal residual stresses are included. As the applied load is increased, the thicker repair becomes more effective than the thinner patch in reducing the stress intensity factor.

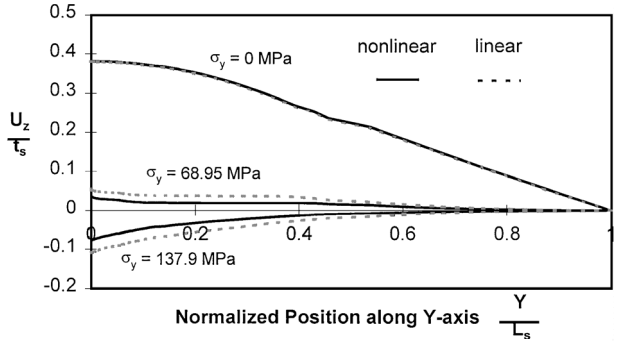

Fig. 6 Curvature of aluminum plate midplane along y axis for eight-ply composite repair.

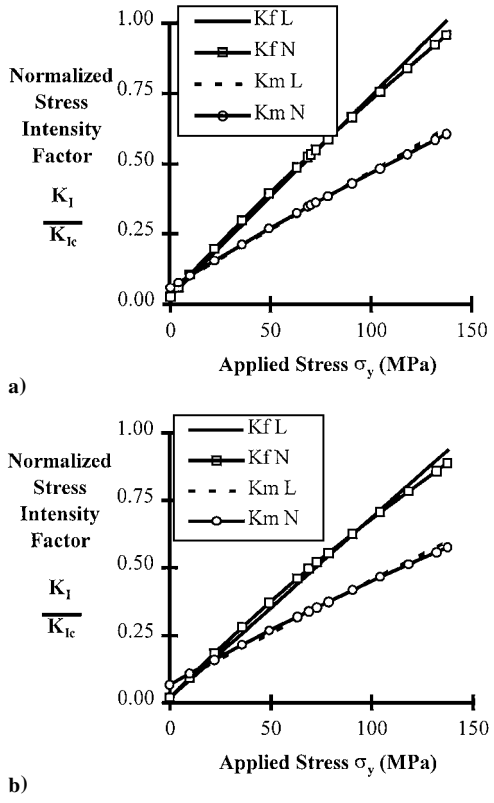

Fig. 7 Normalized stress intensity factor with $\Delta T = -70^{\circ}$C for the a) four-ply and b) eight-ply repairs.

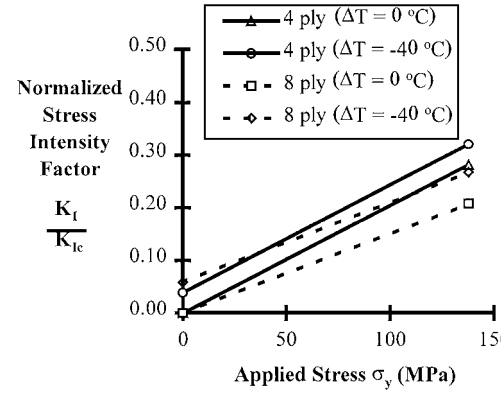

Fig. 8 Normalized stress intensity factor for double-sided repairs.

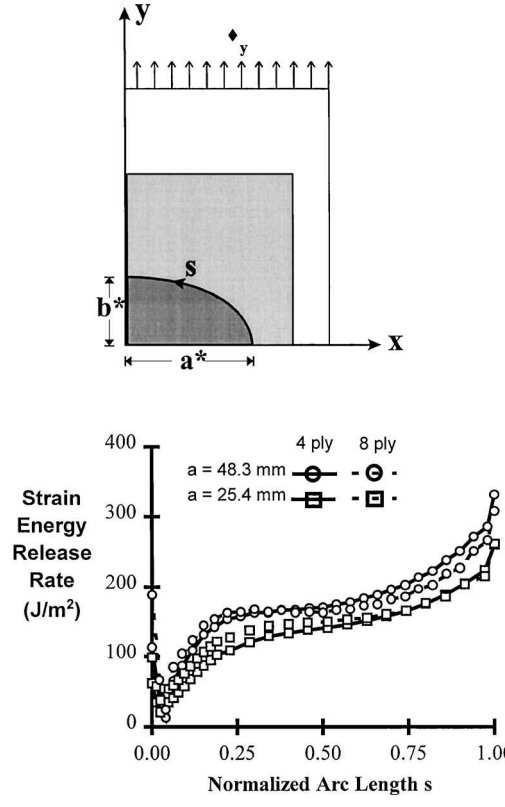

Fig. 9 Debond strain-energy release rate distributions for single-sided repair.

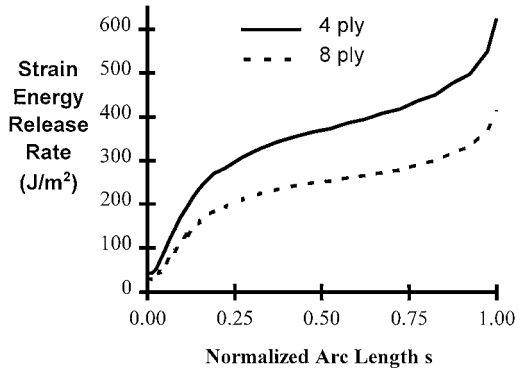

Fig. 10 Debond strain-energy release rate distributions for double-sided repair.

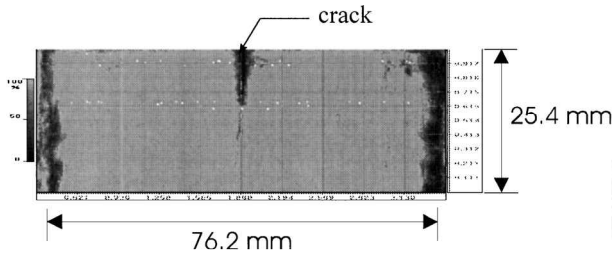

a) $N = 55 \times 10^3$, $a = 26$ mm

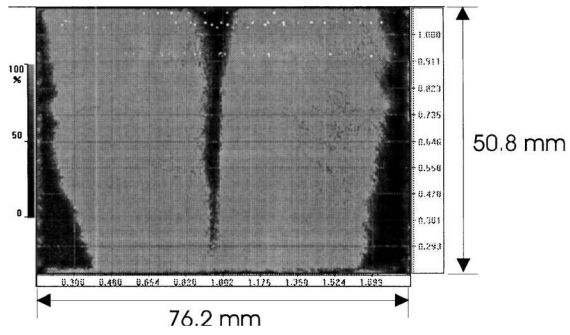

b) $N = 95 \times 10^3$, $a = 48$ mm

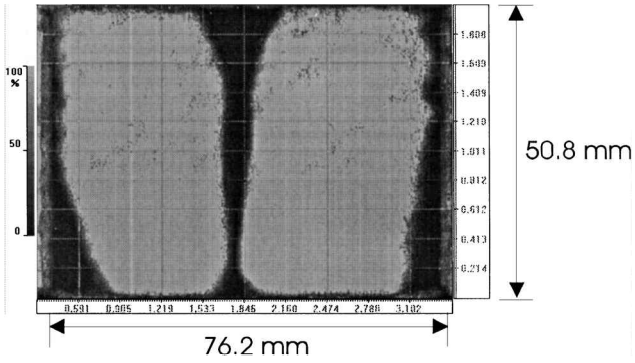

c) $N = 122 \times 10^3$, $a = 62$ mm

Fig. 11 Ultrasonic C-scans of repair area for four-ply single-sided repair with initial crack length of 12 mm and $\Delta\sigma = 68.95$ MPa.

Strain-energy release rate distributions for the single- and the double-sided repairs are shown in Figs. 9 and 10. For this specimen, the debond crack front and aluminum crack front are assumed to coincide. An ellipse with aspect ratio $b^*/a^* = 0.2$ is used to make comparisons of the repair geometries. The strain-energy release rate is plotted from the x axis at the aluminum crack tip to the y axis. Figure 9 shows that for two debond sizes, the distribution of the strain-energy release rate is nearly equal for each of the thick and the thin repairs. Also, the strain-energy release rate increases near the free edge of the edge-cracked specimen. Thus one would expect the greatest debond growth near the free edge. Figure 10 shows that for double-sided repair, the magnitude of the strain-energy release rate is higher for the thin patch. The strain-energy release rate also increases near the free edge of the specimen. Consequently, we see that the debonding characteristics for the single-sided repair are similar for the thick and the thin patches, but are different for the double-sided repair.

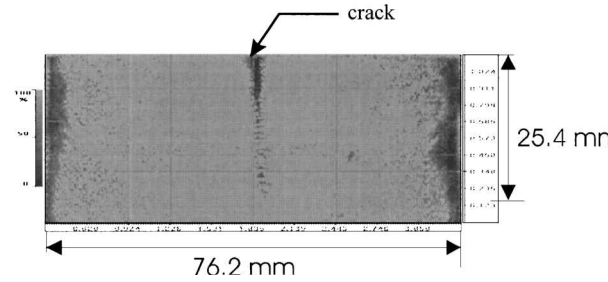

a) $N = 55 \times 10^3$, $a = 25.4$ mm

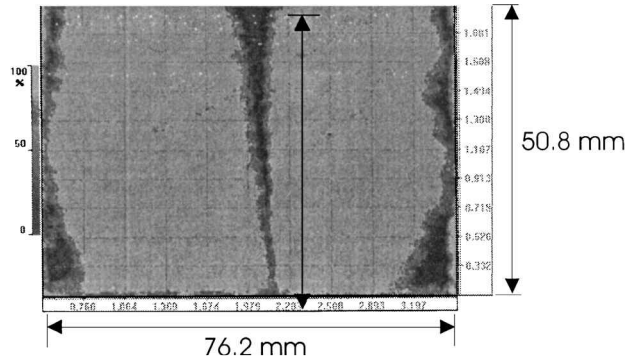

b) $N = 110 \times 10^3$, $a = 51.6$ mm

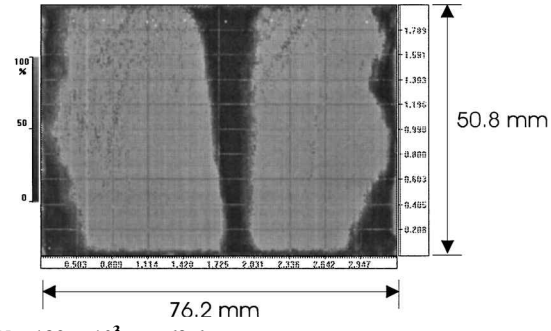

c) $N = 132 \times 10^3$, $a = 69.6$ mm

Fig. 12 Ultrasonic C-scans of repair area for eight-ply single-sided repair with initial crack length of 12 mm and $\Delta\sigma = 68.95$ MPa.

Images of the ultrasonic C-scan are shown in Figs. 11–14. The images are of specimens subjected to fatigue loading, taken at various cycles during the testing. The fatigue stress ranges for the single- and the double-sided repairs are $\Delta\sigma = 68.95$ MPa, $R = 0$ and $\Delta\sigma = 137.9$ MPa, $R = 0$, respectively. Note that no initial tensile load was applied to the specimen in order to minimize the initial transverse deflection in the single-sided repair, as mentioned by Belason[8] and shown in Fig. 6. The number of cycles (10^3) and crack position for the single-sided repair a_f are indicated below the images. The aluminum crack for the single-sided repair is tracked on the reverse side of the repair by an optical microscope. True aluminum crack positions for the double-sided repairs are indicated by open symbols. It is believed that the aluminum fatigue crack is too fine and its crack tip position cannot be accurately measured from the C-scan image. Thus the crack length is indicated by an open symbol to identify the length as an approximate measure.

The images in Figs. 11 and 12 show that the debond growth and the aluminum crack growth for the thin and the thick repairs

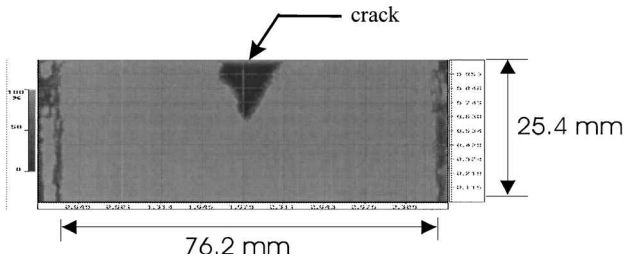

a) $N = 25 \times 10^3$

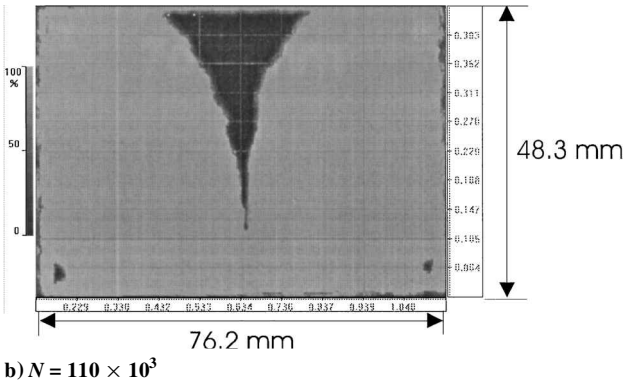

b) $N = 110 \times 10^3$

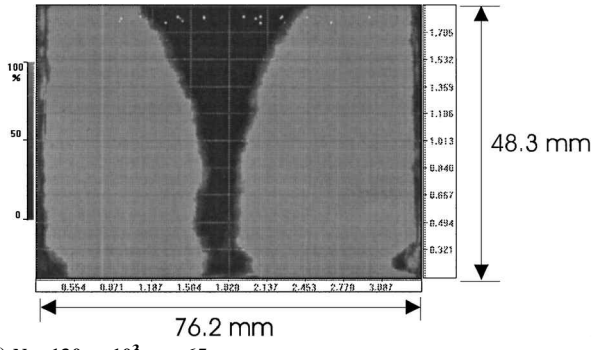

c) $N = 130 \times 10^3$, $a = 65$ mm

Fig. 13 Ultrasonic C-scans of repair area for four-ply double-sided repair with initial crack length of 13.5 mm and $\Delta\sigma = 137.9$ MPa.

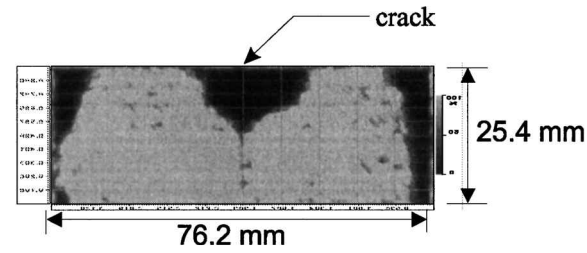

a) $N = 100 \times 10^3$

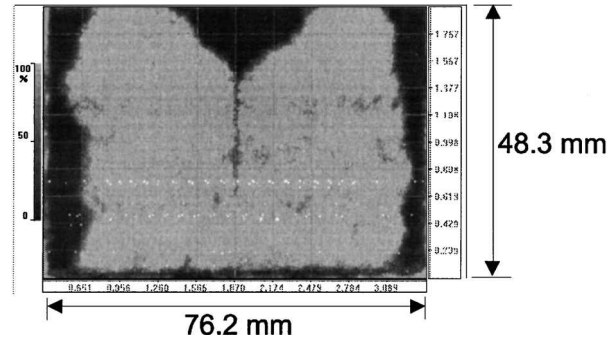

b) $N = 200 \times 10^3$

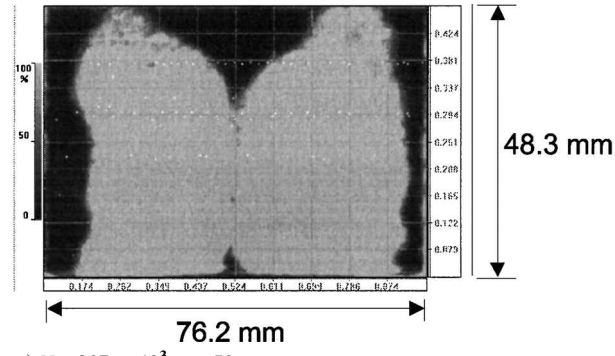

c) $N = 307 \times 10^3$, $a = 52$ mm

Fig. 14 Ultrasonic C-scans of repair area for eight-ply single-sided repair with initial crack length of 13 mm and $\Delta\sigma = 137.9$ MPa.

are similar. It seems that initially the debonding is very small, as shown by the first image in each figure. Also, the debond does not seem to cover the length of the aluminum crack significantly. As the aluminum crack grows outside of the repair edge, as shown in the next image, the debond area increases. However, there does not seem to be significant debonding. In fact, the debonding along the repair edge seems to be as much as that along the aluminum crack. The final image shows the debonding after the aluminum crack has grown a little distance away from the repair edge.

The debonding for the thin and the thick repairs shown in Figs. 13 and 14 appears to be different. The thin repair seems to have more debonding along the aluminum crack over the entire fatigue life, although the thick repair initially has more debonding. Also there is some debonding along the repair edge.

Predictions of the fatigue life are made by numerical integration of a Paris law:

$$N = \int_{a_i}^{a_f} \frac{\mathrm{d}a}{C(\Delta K)^m}$$

where a_i and a_f are the initial and the final aluminum crack lengths, respectively. The material constants[9] used for aluminum 2024-T3 are $C = 4.086 \times 10^{-10}$ and $m = 2.318$. Normally the materials constants are dependent on the R ratio, which is defined as the ratio of the minimum to the maximum applied stresses.

Fatigue life data and predictions for the single-sided repair are shown in Fig. 15. The test data are labeled Test 1 and Test 2. Both repairs increase the fatigue life approximately 3.5 times over that of the nonrepaired specimen. It is immediately apparent that the thicker repair does not significantly improve the fatigue life. $K_{\max}$ (the value of the stress intensity factor at peak applied load) is used instead of ΔK ($K_{\max} - K_{\min}$) for the predictions. Because there is a $K_{\min}$ (the minimum value of the stress intensity factor) at zero load (for $R = 0$) because of the thermal residual stresses, this leads to an effective R ratio. R-ratio-dependent material constants C and m are not currently used for the analysis. The effect of debonding on the stress intensity factor is neglected because it was found that there was not a significant increase in stress intensity until the aluminum crack penetrated the repair. At this point significant debonding occurs as the repair performs like a lap joint. Fatigue life cycle predictions by use of the stress intensity at the free edge N_f, midplane N_m, and root-mean-square value N_{rms} are indicated. Callinan et al.[10] showed the root-mean-square stress intensity factor as follows:

$$K_{\mathrm{rms}} = \sqrt{\frac{1}{t_s}\int_{-t_s/2}^{t_s/2} K^2(z)\,\mathrm{d}z}$$

When Eq. (2) is substituted into $K(z)$, the following equation can be derived:

$$K_{\mathrm{rms}}^2 = K_m^2 + \tfrac{1}{3}K_f^2$$

The prediction with the free edge and the midplane stress intensity factors span the test data. It seems that using K_{rms} to compute the

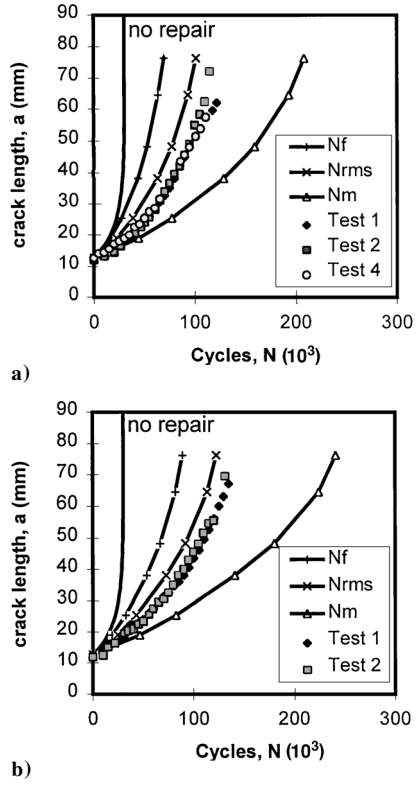

Fig. 15 Crack length *a* vs cycles *n* for single-sided repair with a) four-ply graphite/epoxy and b) eight-ply graphite/epoxy composite.

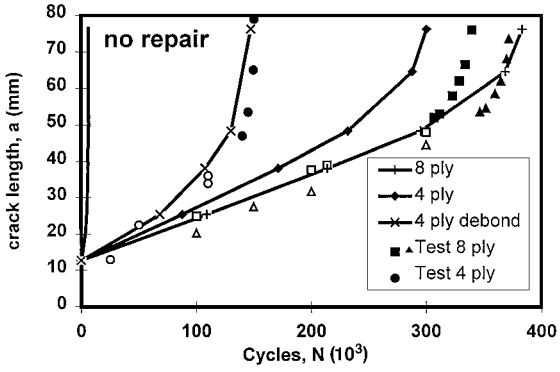

Fig. 16 Crack length *a* vs cycles *N* for double-sided repair.

fatigue life gives a very good conservative prediction for both the thick and the thin repairs.

Figure 16 shows the fatigue life data for the double-sided repairs. The test data are shown only at the point where the fatigue crack penetrates or travels completely through the repair. It is evident that the thicker patch leads to a greater fatigue life. Analysis is performed to predict the number of cycles for the fatigue crack to penetrate the repair. Analysis without debonding can predict the results for the thick, but not the thin, repair. Since the thin patch has significantly more debond growth over the entire aluminum crack length, the effects of debonding on the stress intensity factor are added. The debonding effects were achieved with the assumption of an elliptic debond of approximately the same size as the actual debond from the C-scan image. An ellipse is chosen to approximate the debond front at the location near the crack tip. Note that the debond is actually larger near the free edge. This approximation still leads to conservative predictions of the fatigue life, as shown in the figure.

Conclusions

In this study, bonded composite single- and double-sided patches are investigated. Thermal residual stresses in the aluminum panel induced during bonding can significantly affect the effectiveness of patching and therefore must be accurately determined. Double-sided repairs are much more effective in increasing fatigue life, but may be more difficult to put into practice. Increasing the thickness of a low coefficient of thermal expansion composite like graphite/epoxy may not have a significant effect on fatigue crack growth for single-sided repairs. It seems that $K_{\max}$ can be effectively used to estimate the fatigue life. Debond growth must be taken into account in the stress intensity factor and subsequent fatigue life when there is significant debonding along the aluminum crack. Because the stress intensity factor varies through the thickness for single-sided repairs, the fatigue life is computed with K_{rms}, and this method seems to estimate the fatigue life accurately.

Acknowledgments

This work was supported by the U.S. Air Force Office of Scientific Research through University Research Initiative Grant F49620-93-0377 to Purdue University. Walter Jones was grant monitor.

References

[1] Baker, A. A., and Jones, R., *Bonded Repair of Aircraft Structure*, Martinus Nijhoff, Dordrecht, The Netherlands, 1988.

[2] Chue, C., Chang, L., and Tsai, J., "Bonded Repair of a Plate with Inclined Central Crack Under Biaxial Loading," *Composite Structures*, Vol. 28, 1994, pp. 39–45.

[3] Sun, C. T., Klug, J., and Arendt, C., "Analysis of Cracked Aluminum Plates Repaired with Bonded Composite Patches," *AIAA Journal*, Vol. 34, No. 1, 1996, pp. 369–374.

[4] Young, A., Rooke, D. P., and Cartwright, D. J., "Analysis of Patched and Stiffened Cracked Panels Using the Boundary Element Method," *International Journal of Solid Structures*, Vol. 29, 1992, pp. 2201–2216.

[5] Baker, A., "Growth Characterization of Fatigue Cracks Repaired with Adhesively Bonded/Epoxy Patches," *Proceedings of the 9th International Conference on Fracture, Advances in Fracture Research*, edited by B. L. Karihaloo, Y.-W. Mai, M. I. Ripley, and R. O. Ritchie, Pergamon, New York, Vol. 1, 1977, pp. 117–128.

[6] Klug, J., and Sun, C. T., "Large Deflection Effects of Cracked Aluminum Plates Repaired with Bonded Composite Patches," *Proceedings of the First International Conference on Composite Science and Technology*, Durban, South Africa, June 1996.

[7] Rybicki, E., and Kanninen, M., "A Finite Element Calculation of Stress Intensity Factors by a Modified Crack Closure Integral," *Engineering Fracture Mechanics*, Vol. 9, 1977, pp. 931–938.

[8] Belason, E., "Fatigue and Static Ultimate Tests of Boron/Epoxy Doublers Bonded to 7075-6 Aluminum with a Simulated Crack," *18th Symposium of the International Conference on Aeronautical Fatigue*, Melbourne, Australia, May 1995.

[9] Phillips, P., "Long Crack Growth Rate Data—Constant Amplitude and FALSTAFF Loading," *Short-Crack Growth Behavior in an Aluminum Alloy*, edited by J. C. Newman, Jr., and P. R. Edwards, AGARD Cooperative Test Programme, Rept. 732, AGARD, 1988, pp. 78–83.

[10] Callinan, R. J., Rose, L. R. F., and Wang, C. H., "Three Dimensional Stress Analysis of Crack Patching," *Proceedings of the 9th International Conference on Fracture, Advances in Fracture Research*, edited by B. L. Karihaloo, Y.-W. Mai, M. I. Ripley, and R. O. Ritchie, Pergamon, New York, Vol. 1, 1977, pp. 2151–2158.